# L-subshell ionization of Au, Tl, Pb, Bi, Th, and U by protons*

C. V. Barros Leite, N. V. de Castro Faria, and A. G. de Pinho

*Department of Physics, Catholic University, Rio de Janeiro, Brazil* †

(Received 5 October 1976)

L-subshell ionization cross sections for Au, Tl, Pb, Bi, Th, and U by proton impact have been determined over the projectile range 0.5–3.5 MeV. The measured x-ray production cross sections of the total L shell and of some well resolved lines or groups of lines are consistent with those obtained by different authors in the same regions of bombarding energies and atomic numbers. Ionization cross sections were obtained by using the above results and experimental values for the relative radiative transition probabilities, fluorescence yields, and Coster-Kronig factors. The branching ratios of radiative transitions were measured and are in good agreement with the widely used theoretical calculations of Scofield, Rosner, and Bhalla. The values of fluorescence and Coster-Kronig yields were taken from previously published experiments performed in our laboratories. The influence of these experimental data on the shape of cross section versus proton energy curves is discussed. Comparisons of the experimentally determined L-subshell ionization cross sections are made with calculations in the plane-wave Born (PWBA), semiclassical, and binary-encounter approximations. The large effect of binding-energy, trajectory, and relativistic corrections on the PWBA calculations invalidates quantitative conclusions regarding agreement between experimental and theoretical values. Semiclassical arguments are presented, however, to explain some general aspects of the ionization cross-section curves.

## I. INTRODUCTION

The study of atomic inner-shell ionization by the impact of heavy charged particles is important for two reasons. On the one hand, it sheds more light on atomic structure and atomic-ion collision mechanisms,[1] and on the other hand, there are many practical applications of characteristic x-ray analysis[2] for which precise cross sections are needed. K-shell ionization has been extensively studied experimentally and results have been published[3] showing good agreement with current theoretical models in the case of light incident ions (protons and helium ions). With the development of cooled semiconductor detectors, the x-ray lines following the filling of vacancies in the closely spaced L subshells of heavy elements could be fairly well resolved, and a broad research field was opened up.

However, to go from the directly measured intensities of L x rays to the ionization cross sections $\sigma_I^{Li}$ of each subshell ($i = 1, 2, 3$) is not simple. In fact, acknowledgment of relative radiative decay rates, fluorescence yields, and Coster-Kronig factors is required. Calculations by Scofield[4, 5] and Rosner and Bhalla[6] on the rates of emission of x rays from each L subshell are available, but precise and systematic measurements of these rates are still lacking. Fluorescence yields and Coster-Kronig and experimental[9] results exhibit large discrepancies, complicating the choice of a coherent set of values. A systematic experimental determination of these coefficients for some heavy elements ($Z \geq 81$) was performed in our laboratories[10-13] and values obtained by interpolation on a smooth curve fitting the experimental points were used together with our measured branching ratios to obtain the ionization cross sections from the raw L x-ray data. An analysis of the importance of these factors on the absolute values of ionization cross sections and on the shape of the $\sigma_I^{Li}(E)$ curves is worthwhile before a comparison with the theoretical predictions.

L-subshell ionization cross sections by energetic protons have been calculated in the plane-wave Born approximation (PWBA), binary-encounter approximation (BEA), and semiclassical approximation (SCA). Several investigators as, for example, Datz et al.[14] and Tawara et al.,[15] show some discrepancies between experimental and PWBA values. Although simple hydrogenic wave functions are used in PWBA calculations, some authors thought that discrepancies were due to the fact that the hyperbolic trajectory of the proton and the effect of the changing binding energy of the target electrons (slow collisions), were generally not taken into account. Brandt and Lapicki[16] analyzed the binding energy effect in L-shell ionization and also suggested a correction factor for the Coulomb deflection of the projectile. These corrections were included by Pepper[17] in his XCODE computer program and can be compared with experimental values.

An important aspect of the theoretical PWBA ionization cross sections of the $L_1$ subshell is the plateau that appears in the region of proton energy

of 1–2 MeV for heavy elements. This plateau is also predicted by the SCA[18] and by the recent BEA calculations of McGuire and Omidvar.[19] Two preliminary questions must be answered: first, if these inflections appear in experimental curves and, second, if there is some correlation between the position of the plateau and the atomic number of the target. Hasteen[18] proposed an explanation for the origin of the plateau based on semiclassical arguments: the main contribution to the ionization cross sections comes from a region around a particular impact parameter. As the incident projectile energy increases, this region of dominant impact parameter is higher and crosses the node of the $2s_{1/2}$ electron wave function. Thus, it would be possible to interpret the plateau as a manifestation of this node. Measurements of $L$ x-ray yields from atoms with different $Z$ values and calculations of the corresponding $2s_{1/2}$ node can be a qualitative test of this explanation. A few years ago Kingston[20] advanced similar arguments showing that, in the framework of the impulse approximation, a density node in velocity space would correspond to a flattening of the cross section vs bombarding energy curve. Since the BEA may be regarded as a special case of the impulse approximation, it is not surprising that the same effects were obtained by McGuire and Omidvar[19] with a convenient transformation of the density distributions from velocity to coordinate space.

In this paper we treat collisions between protons (0.5–3.5 MeV) and Au, Tl, Pb, Bi, Th, U targets, with subsequent $L$ x-ray production. Two kinds of experiments were performed for each subshell, namely, the measurement of radiative decay branching ratios, and the x-ray production cross section dependence on the proton energy. Ionization cross sections are extracted from the data and compared with presently available theories. All relevant features mentioned in this introduction are discussed.

## II. EXPERIMENTAL PROCEDURES AND ANALYSIS OF DATA

Targets with a thickness of approximately 50 $\mu$g/cm$^2$ were prepared by vacuum evaporation of Tl, Pb, and Bi onto thin Formvar films and Th and U onto 100-$\mu$g/cm$^2$ Al backing foils. The Au foil was self-supporting. The PUC/RJ 4-MV Van de Graaff accelerator provided the proton beam. Currents were typically 30–200 nA to avoid extreme dead time and electronic pile up problems. The thickness of the targets was determined and monitored during the data acquisition using Rutherford scattering of the proton through 90°. The target thickness was always kept small in order to minimize proton energy loss and self-absorption of the x rays in the target. Both effects were neglected in the following. The x rays were detected by a Si (Li) detector with a measured resolution of 190 eV at 6.4 keV. The detector was positioned outside the target chamber at an angle of 90° to the incident beam direction. The vacuum separation was maintained by a 4-mm-diam Mylar window 6 $\mu$m thick. A thin Al foil in front of the detector was used to attenuate the strong $M$ x rays, thus reducing pile-up effects. Targets were oriented at 45° with respect to the beam and were mounted on a rotating disk with six positions to facilitate target changing. The scattered protons were detected by a surface barrier detector whose solid angle was measured carefully. A Faraday cup and a digital integrator permitted the calculation of the number of protons incident on the target during each run. Standard electronic modules were used. Figure 1 shows two statistically good spectra ($\sim 10^7$ counts in the integrated $L$ spectrum) of Au and U obtained at a bombarding energy of 2 MeV and used for branching ratio measurements. It can be seen that the average separation of the $L$ x-ray lines increases with the atomic number. In particular, one may note that the $L_\beta$ group is not resolved for Au while for U the lines $\beta_{2, 15}$ ($L_3N_{4, 5}$) and $\beta_1(L_2M_4)$ are well defined. Thus, more precision should be expected measuring branching ratios for higher-$Z$ elements. However, due to energy crossings, some of the more intense lines of high-$Z$ spectra are less well defined than in the spectra of lower-$Z$ elements. Typical examples are the transitions $\eta(L_2M_1)$ and $\beta_5(L_3O_{4, 5})$.

A detailed description of the detection system and the method used in the analysis of the spectra is presented elsewhere.[10-13] Since most of the individual lines in the $L_\alpha$, $L_\beta$, and $L_\gamma$ groups are not fully resolved, a peak fitting procedure has to be used to extract accurate values for the intensities of the lines. A graphical stripping method was employed and full energy peak profiles were determined experimentally for different portions of the spectra. These standard peaks were $K_\alpha$ lines of light elements obtained by proton impact and decomposed into their two components by a graphical iterative procedure. The variation of the FWHM was observed to be fairly linear with the proton energy within the limited range of interest and so was determined by interpolation from the measured standards. The form of the low-energy tail of the peak was carefully determined for each interval of approximately 3 keV.

For the determination of cross sections of all the elements under investigation, it was enough to consider the well defined lines $\gamma_1(L_2N_4)$, $\gamma_4(L_1O_{2, 3})$,
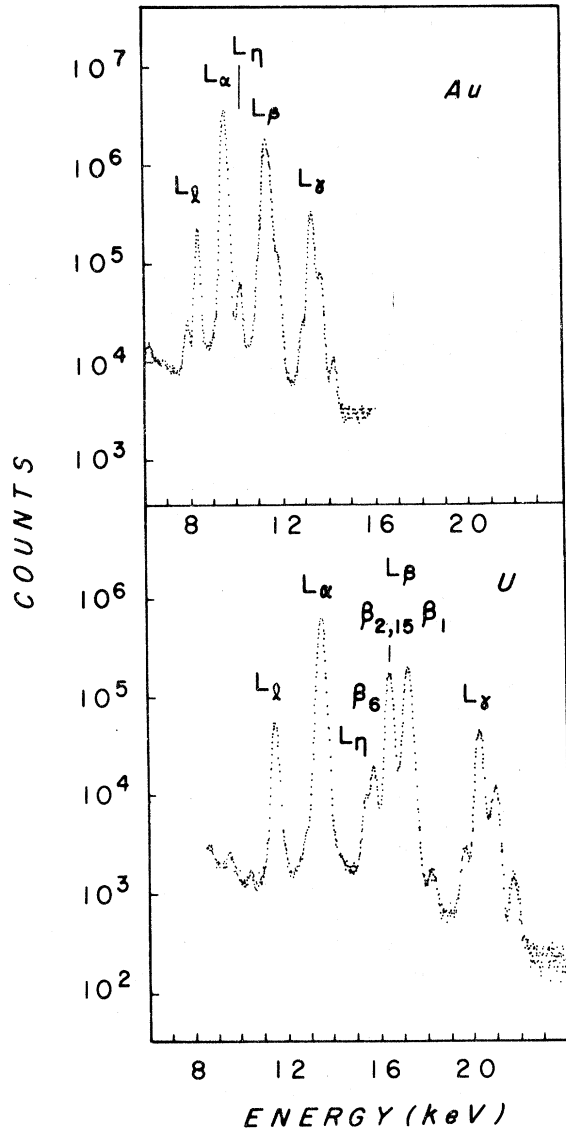
FIG. 1. Au and U *L* x-ray spectra obtained by 2-MeV proton impact.

and $\alpha_{1,2}(L_3M_{5,4})$, where the errors are essentially of statistical origin.

In the branching ratio measurements it is necessary to know the relative efficiency of the x-ray detection system, including the intrinsic efficiency as well as x-ray attenuation by the Mylar window, air path, Al absorber and Be entrance window. *K* x rays produced by proton impact on light elements and gamma rays from standard calibrated radioactive sources were employed. The sources were mounted in the chamber at the target location and therefore had a geometry representative of the actual experimental conditions. In the cross-sec-

tion calculations the charge collected in the Faraday cup and the number of protons Rutherford scattered elastically by each element were also recorded for normalization. The absolute efficiency of the x-ray detection system, including the solid angle subtended by the detector, was obtained with a calibrated point source of $^{109}$Cd. In all the calculations the radiation was assumed to be emitted isotropically.

## III. RESULTS

### A. *L* x-ray production cross sections

The ionization cross sections $\sigma_I^{Li}$ can be written as an explicit function of the x-ray production cross sections $\sigma_x^k$. As previously observed, we chose three representative transitions to measure the x-ray yields from each one of the *L* subshells, namely, $\gamma_4$, $\gamma_1$, and $\alpha_{1,2}$ $(\equiv \alpha)$. This choice reflects the fact that they are the easiest lines to pick out among the $L_1$, $L_2$, and $L_3$ lines, respectively. Then

$$\sigma_I^{L1} = \sigma_x^{\gamma_4} \left( \frac{1}{\omega_1} \right) \frac{\Gamma_1}{\Gamma_1^{\gamma_4}} \qquad (1)$$

$$\sigma_I^{L2} = \sigma_x^{\gamma_1} \left( \frac{1}{\omega_2} \right) \frac{\Gamma_2}{\Gamma_2^{\gamma_1}} - f_{12}\sigma_x^{\gamma_4} \left( \frac{1}{\omega_1} \right) \frac{\Gamma_1}{\Gamma_1^{\gamma_4}}, \qquad (2)$$

$$\sigma_I^{L3} = \sigma_x^{\alpha} \left( \frac{1}{\omega_3} \right) \frac{\Gamma_3}{\Gamma_3^{\alpha}} - f_{23}\sigma_x^{\gamma_1} \left( \frac{1}{\omega_2} \right) \frac{\Gamma_2}{\Gamma_2^{\gamma_1}}$$

$$- f_{13}\sigma_x^{\gamma_4} \left( \frac{1}{\omega_1} \right) \frac{\Gamma_1}{\Gamma_1^{\gamma_4}}, \qquad (3)$$

where $\omega_i$ is the fluorescence yield of the *i* subshell, $f_{ij}$ are the Coster-Kronig factors describing the nonradiative transfer of vacancies from the *i* to the *j* subshell, $\Gamma_i$ is the total radiative width and $\Gamma_i^k$ is the partial radiative width for the *K* transition of the *i* subshell. Obviously,

$$\sigma_x^{Li} = \sigma_x^k \left( \Gamma_i / \Gamma_i^k \right).$$

For thin targets, the absolute *k*-line production cross section as function of the proton energy *E* is given by

$$\sigma_x^k(E) = \frac{N_x^k}{(1 - \tau)\epsilon N_c N_a} \qquad (4)$$

where $N_x^k$ is the measured number of counts in *k* line, $\tau$ is the fractional dead time (in general less than 5%), $\epsilon$ is the overall efficiency of the x-ray spectrometer at the energy of the *k* line, and $N_c$ is the number of protons collected in the Faraday cup. The surface target density, $N_a$ (in atoms /cm$^2$), is obtained from the expression

$$N_a = \frac{N_p}{\Omega_p N_c (d\sigma/d\Omega)_R}, \qquad (5)$$

TABLE I. X-ray production cross sections $\sigma_x^{L\alpha}$ and $\sigma_x^L$ (total). Data from Refs. 15 and 24 were obtained by graphical interpolation to our energy values.

| $\sigma_x$ (barn) | 0.5 | 1.0 | 1.5 | 2.0 | 2.5 | 3.0 | 3.5 | Reference |
|---|---|---|---|---|---|---|---|---|
| | | | Proton energy (MeV) | | | | | |
| Au $\sigma_x^{L\alpha}$ | 0.39±0.03 | 3.65±0.25 | 9.2±0.6 | 18.1±1.3 | 28.7±2.0 | 38.8±2.7 | | This work |
| | | 2.7 | | | | 32 | | 21 |
| | | 4.5 | 10.8 | 20.5 | 29.5 | 48±8 | | 15 |
| $\sigma_x^L$ | 0.67±0.05 | 6.2±0.4 | 15.8±1.1 | 32.0±2.2 | 51.1±3.6 | 70.2±5.0 | | This work |
| | 0.45±0.4 | 4.52±0.39 | 13.6±1.1 | 28.4±2.4 | 43.5±3.7 | 60.9±5.3 | | 22 |
| | | 7.6 | 18.4 | 33.3 | 49.4 | 76.2 | | 15 |
| | | | 14.5 | 30.7 | 54.0 | 77.4 | | 23 |
| | | 4.51±0.98 | 12.7±2.9 | 24.7±5.6 | 39.9±9.1 | 57±13 | 76±17 | 33 |
| | | 11.6±2.3 | | 27.0±5.4 | 48.0±9.6 | 74±15 | 96±19 | 34 |
| Tl $\sigma_x^{L\alpha}$ | 0.33±0.02 | 2.97±0.21 | 9.66±0.68 | 16.5±1.2 | 27.0±1.9 | 33.5±2.3 | | This work |
| $\sigma_x^L$ | 0.57±10.04 | 5.1±0.4 | 16.6±1.2 | 29.1±2.0 | 48.1±3.4 | 60.9±4.3 | | This work |
| Pb $\sigma_x^{L\alpha}$ | 0.22±0.02 | 2.20±0.2 | 6.85±0.48 | 13.5±1.0 | 21.9±1.5 | 31.7±2.2 | 41.2±2.9 | This work |
| | | 1.8±0.3 | | | | 24±4 | | 21 |
| | | | | 14.7 | | 32.5 | | 24 |
| $\sigma_x^L$ | 0.37±0.03 | 3.70±0.3 | 11.7±0.8 | 23.4±1.6 | 38.7±2.7 | 57.1±4.0 | 74.4±5.2 | This work |
| | | 3.9±0.4 | | 26.6±4.0 | | 58.6±8.8 | | 24 |
| | | | 10.6±0.3 | 24.3±0.7 | 35.9±1.1 | 51.7±2.0 | | 23 |
| | | 3.84±0.54 | 11.2±1.5 | 21.9±2.9 | 36.0±5.0 | 53.7±7.5 | | 35 |
| | | | 9.1±1.8 | 24.0±4.8 | 42.0±8.4 | 54±11 | 76±15 | 34 |
| Bi $\sigma_x^{L\alpha}$ | 0.180±0.01 | 2.40±0.17 | 6.64±0.46 | 11.9±0.8 | 19.5±1.4 | 27.0±1.9 | | This work |
| | | 1.6 | | | | 22 | | 21 |
| | | 2.83 | 7.28 | 12.2 | 19.1 | 30.6±5.7 | | 15 |
| $\sigma_x^L$ | 0.321±0.02 | 4.33±0.30 | 11.9±0.8 | 23.4±1.6 | 36.1±2.5 | 50.9±3.6 | | This work |
| | | 5.6 | 12.7 | 24.0 | 34.5 | 52.2±10 | | 15 |
| | | 2.38±0.54 | 7.8±1.7 | 15.8±3.6 | 26.6±6.0 | 38.7±8.8 | 52±11 | 33 |
| Th $\sigma_x^{L\alpha}$ | 0.085±0.006 | 1.07±0.07 | 3.78±0.26 | 8.13±0.57 | 13.0±0.9 | 18.7±1.3 | | This work |
| | | 0.72 | 2.3 | 4.8 | 8.2 | 12 | | 21 |
| $\sigma_x^L$ | 0.160±0.01 | 1.88±0.13 | 6.64±0.46 | 14.3±1.0 | 23.4±1.6 | 33.9±2.4 | | This work |
| U $\sigma_x^{L\alpha}$ | 0.054±0.004 | 0.685±0.050 | 2.55±0.18 | 5.37±0.38 | 9.00±0.6 | 14.0±1.0 | | This work |
| | | 0.55 | | | | 10.0 | | 21 |
| | | 0.92 | 2.57 | 5.14 | 8.23 | 12.0±3 | | 15 |
| $\sigma_x^L$ | 0.094±0.006 | 1.17±0.08 | 4.37±0.31 | 9.32±0.15 | 15.7±1.1 | 25.0±1.8 | | This work |
| | | | 4.4 | 8.8 | 15.0 | 22±4 | | 15 |
| | | | 3.4±0.7 | 9.0±1.8 | 16.5±3.3 | 24.0±4.8 | | 34 |
| | | | | 19.1±1.0 | 33.8±1.6 | 47.7±2.3 | 64.8±3.2 | 36 |

where $(d\sigma/d\Omega)_R$ is the differential cross section for Rutherford scattering of protons at 90° laboratory angle, $\Omega_p$ is the solid angle subtended by the proton detector, and $N_p$ is the number of protons scattered by the target element recorded by scalers after the electronic signal passed through a pulse height discriminator. By accumulating the x ray and proton spectra simultaneously, the incident beam flux and the number of target atoms may be cancelled out. The resulting expression is

$$\sigma_x^k(E) = \left(\frac{d\sigma}{d\Omega}\right)_R \frac{N_x^k}{N_p} \frac{\Omega_p}{(1-\tau)\epsilon} . \qquad (6)$$

The total $(\sigma_x^T)$ and $L_{\alpha1,2}$ $(\sigma_x^\alpha)$ x-ray productions

cross sections for the six elements which were investigated are presented in Table I. The errors indicated in the table come mainly from the measurements of the particle detector solid angle and x-ray detector efficiency, the statistical errors from counting being small. Some known results from other authors are also shown, the agreement being generally good.

### B. Branching ratios

Considerable effort was spent in the experimental determination of the branching ratios. Detailed results discussed together with other values measured by us and covering a wide range of

TABLE II. The relevant $\Gamma_i^k/\Gamma_i^m$ ratios used in the determination of the $\sigma_I^{Li}$ cross sections compared with theoretical (Refs. 4 and 5) predictions and experimental values from the compilation of Ref. 26.

| Branching | Element | | | | | | |
| ratio | Au | Tl | Pb | Bi | Th | U | Reference |
|---|---|---|---|---|---|---|---|
| $\Gamma_1^{\gamma4}/\Gamma_1$ | $0.034 \pm 0.004$ | $0.042 \pm 0.005$ | $0.035 \pm 0.004$ | $0.033 \pm 0.004$ | $0.053 \pm 0.006$ | $0.049 \pm 0.006$ | This work |
| | 0.034 | 0.037 | 0.038 | 0.040 | 0.048 | 0.050 | 4,5 |
| $\Gamma_2^{\gamma1}/\Gamma_2$ | $0.186 \pm 0.010$ | $0.207 \pm 0.012$ | $0.177 \pm 0.011$ | $0.200 \pm 0.012$ | $0.161 \pm 0.009$ | $0.169 \pm 0.010$ | This work |
| | 0.157 | 0.160 | 0.161 | 0.162 | 0.170 | 0.173 | 4,5 |
| | 0.169 | 0.173 | 0.174 | 0.172 | 0.180 | 0.181 | 26 |
| $\Gamma_3^{\alpha}/\Gamma_3$ | $0.740 \pm 0.037$ | $0.749 \pm 0.037$ | $0.768 \pm 0.038$ | $0.751 \pm 0.038$ | $0.755 \pm 0.038$ | $0.731 \pm 0.037$ | This work |
| | 0.787 | 0.782 | 0.776 | 0.774 | 0.755 | 0.750 | 4,5 |
| | 0.775 | 0.765 | 0.778 | 0.757 | 0.735 | 0.733 | 26 |

atomic numbers will be published in a forthcoming paper.[25] In Table II the relevant $\Gamma_1^{\gamma4}/\Gamma_1$, $\Gamma_2^{\gamma1}/\Gamma_2$ and $\Gamma_3^{\alpha}/\Gamma_3$ ratios are shown and compared with the theoretical predictions of Scofield[4,5] and the values of Salem and Schultz[26] obtained by a least-squares fit to the experimental data available then. We have already commented that the errors in the three selected lines ($\gamma_4$, $\gamma_1$, and $\gamma_\alpha$) are essentially of statistical nature. However, in order to get the ratios, the number of x rays in all lines must be measured since

$$\frac{\Gamma_i^k}{\Gamma_i} = \left( \sum_m \frac{\Gamma_i^m}{\Gamma_i^k} \right)^{-1} .$$

In these cases the sources of error come mainly from background subtraction and the peak-fitting procedure. Statistical errors from counting are generally negligible. The errors presented were estimated as the maximum deviation from the average intensity of each peak in various trials of the fitting process. Some weak lines or some lines not so weak but with an energy such that they are in the neighborhood of very strong ones were not measured experimentally. For these lines we used Scofield's results, which should not change the relevant branching ratios by more than 2–3% except perhaps in the $L_1$ branching ratio of lower-$Z$ elements.

### C. Fluorescence yields and Coster-Kronig factors

The $L$-subshell fluorescence ($\omega_i$), Coster-Kronig ($f_{ij}$), and Auger ($a_i$) yields have been intensively analyzed by one of us[10-13] and results of these works are shown in Fig. 2. The solid curves fitted to the experimental points were used to interpolate values of the coefficients. Although the measurement of experimental points of Fig. 2 is well described in the literature quoted, we present a resume of the principal features of these experiments.

The Bi and Np $L$ x-ray spectra were obtained from the decay of $^{210}$Pb and $^{241}$Am, respectively. It was assumed that all primary $L$ vacancies were produced by internal conversion. There are, in this kind of experiment, six independent coefficients to be calculated, because the original nine factors have to satisfy three independent normalization relations. These six unknown quantities were calculated from the intensities of the unconverted $\gamma$ rays, the intensities of the $L$ x-ray lines, the $L$ subshell internal conversion coefficients,
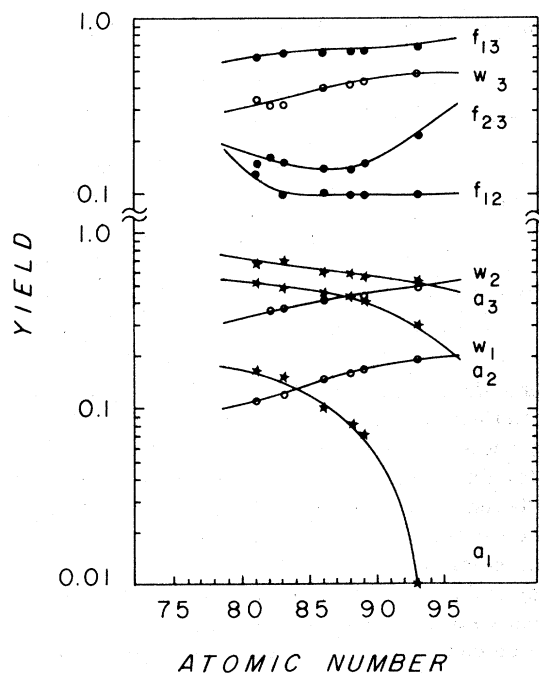


FIG. 2. Experimental values of the fluorescence, Coster-Kronig, and Auger yields reported in Refs. 10–13. The solid curves were used for interpolation in the $Z$ values of interest.
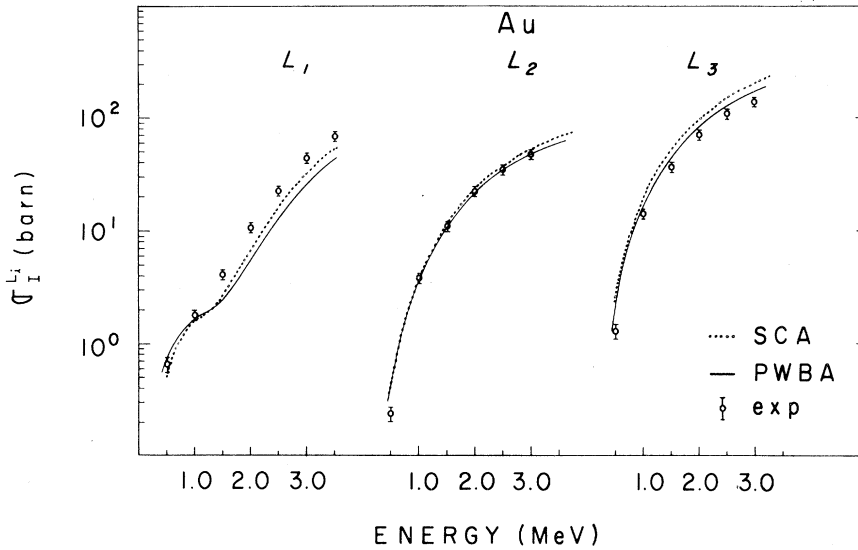
FIG. 3. Experimental ionization cross sections (open circles) for Au vs proton energy. Also presented: PWBA and SCA theoretical curves.

and available information on the Auger electrons yields.

Sources of [231]Pa, free of descendents, were obtained in a column separator and employed to study the Ac $L$ x rays. In the Tl data, the [212]Pb sources were collected electrostatically from the decay products of [220]Rn that emanated from a [228]Th source. An x-ray spectrometer was used to observe $L$ x rays in coincidence with $\gamma$ rays in the first case and with $\alpha$ particles in the second one.

In the Rn and Ra data, a different procedure was employed. The $L$ x-ray spectra come from the internal conversion of the electric quadrupole transitions following the $\alpha$ decay of [226]Ra and [230]Th, respectively. Interpolated values of the $\omega$ and $f$ factors were adopted from the literature. With these values, the internal conversion coefficients of the $E2$ transitions were deduced. Since $E2$ internal conversion coefficients, when measured with good precision are always in excellent agreement with the theory (and this was also true for the $E2$ transitions under consideration in Ra and Rn), the theoretical internal conversion coefficients were adopted and the $\omega$ and $f$ factors deduced. Despite the simple procedure employed to choose the relevant values of the fluorescence and Coster-Kronig yields, the agreement with theoretical predictions for the Auger factors suggest that the resultant values for $\omega_2$ and $\omega_3$ are good within about 5–10%.

The interpolated values of the fluorescence, Coster-Kronig, and Auger yields of Au, Pb, Th, and U were obtained from Fig. 2. The curves are very smooth except for $f_{23}$ in the high-$Z$ region and for $f_{12}$ in the low-$Z$ region. Although it is difficult to decide about the best interpolation in these

cases, the interpolated coefficients satisfy the normalization relations to better than 2% in all the cases. The extrapolation of the $f_{12}$ value for gold is supported by a recent work of Salgueiro et al.[27]

## IV. IONIZATION CROSS SECTIONS AND DISCUSSION

When the measured x-ray cross sections, the branching ratios and the fluorescence and Coster-Kronig factors are introduced in the expressions (1), (2), and (3), we obtain the ionization cross sections (Figs. 3–8). Since most of the systematic errors involved in measurements of the x-ray yields can be eliminated by working with cross-section ratios and to show more clearly the importance of the energy independent coefficients in the expressions for the $\sigma_I^{Li}$, we express (1), (2), and (3) as

$$\frac{\sigma_I^{L2}}{\sigma_I^{L1}} = \omega_{12}\Gamma_{21}\Gamma^{\gamma_4\gamma_1}\frac{\sigma_x^{\gamma_1}}{\sigma_x^{\gamma_4}} - f_{12} \,, \tag{6}$$

$$\frac{\sigma_I^{L3}}{\sigma_I^{L1}} = \omega_{13}\Gamma_{31}\Gamma^{\gamma_4\alpha}\frac{\sigma_x^{\alpha}}{\sigma_x^{\gamma_4}}$$

$$- \omega_{12}\Gamma_{21}\Gamma^{\gamma_4\gamma_1}f_{23}\frac{\sigma_x^{\gamma_1}}{\sigma_x^{\gamma_4}} - f_{13} \,, \tag{7}$$

where the following notation was adopted:

$$\omega_{ij} = \omega_i/\omega_j, \quad \Gamma_{ij} = \Gamma_i/\Gamma_j, \quad \Gamma^{km} = \Gamma_i^k/\Gamma_j^m \,.$$

The $E$ independence of the coefficients is supported by the fact that multiple ionization effects are not expected for protons in the range of energy under consideration. This was verified in the present work by measuring some selected branching ratios as a function of the proton energy. They are constant within the experimental errors.
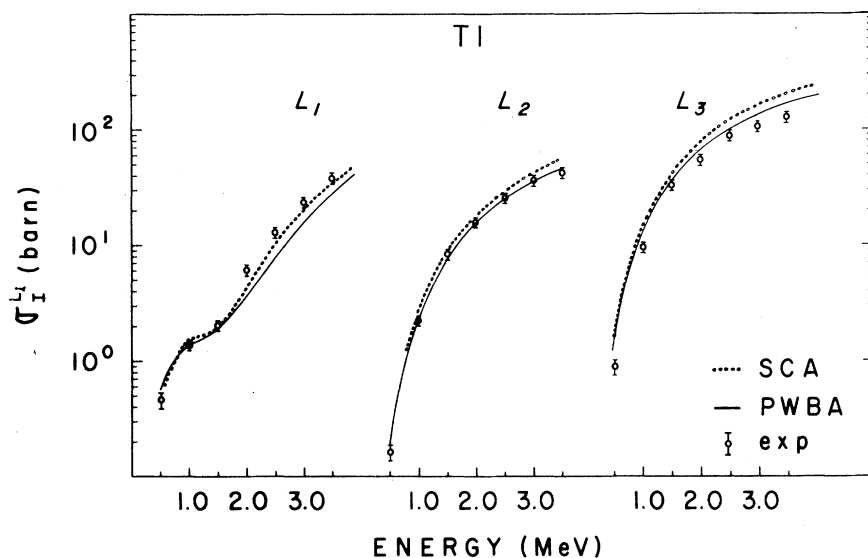
FIG. 4. Experimental ionization cross sections (open circles) for Tl vs proton energy. Also presented: PWBA and SCA theoretical curves.

Our values of ionization cross section ratios are presented in Fig. 9.

When $\sigma_I^{L_3}/\sigma_I^{L_2}$ is compared with the PWBA prediction, experimental and theoretical curves appear to be displaced. Similar results were obtained by Chang _et al._[30] Except for the bismuth data, a somewhat regular increase of the displacement factor with $Z$ is observed. This relatively uniform displacement attains a factor of 2 for Th and U. It is impossible to remove such a discrepancy by

using physically acceptable $\omega$ and $f$ coefficients. Since the corrections due to deflection and binding energy should not be very different in $2p_{1/2}$ and $2p_{3/2}$ subshells, a possible explanation is the $Z$-dependent relativistic correction. In the high-$Z$ atoms, inner-shell electrons should be treated using relativistic wave functions. A relativistic treatment of $L$-shell ionization in the framework of the PWBA has been given by Choi[28] for some elements. For energies below 1 MeV and for gold
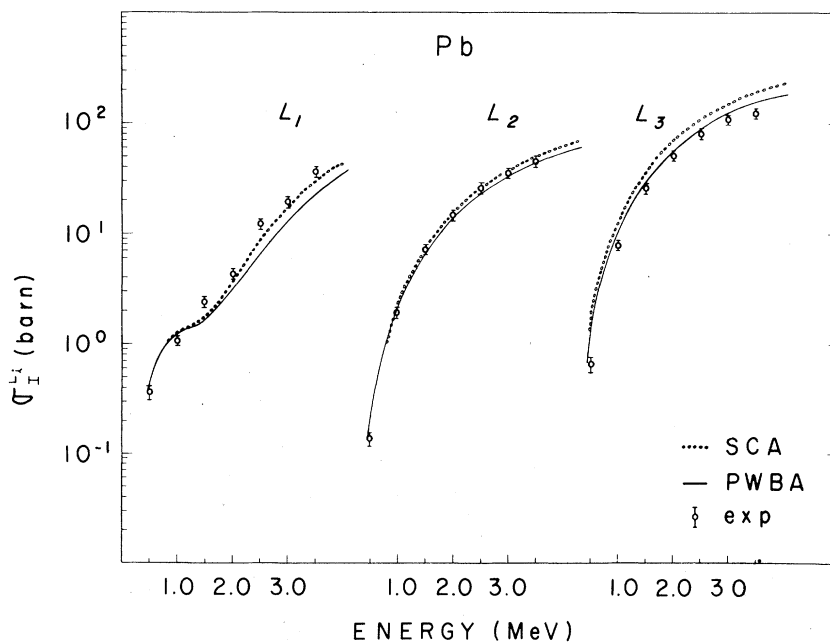


FIG. 5. Experimental ionization cross sections (open circles) for Pb vs proton energy. Also presented: PWBA and SCA theoretical curves.
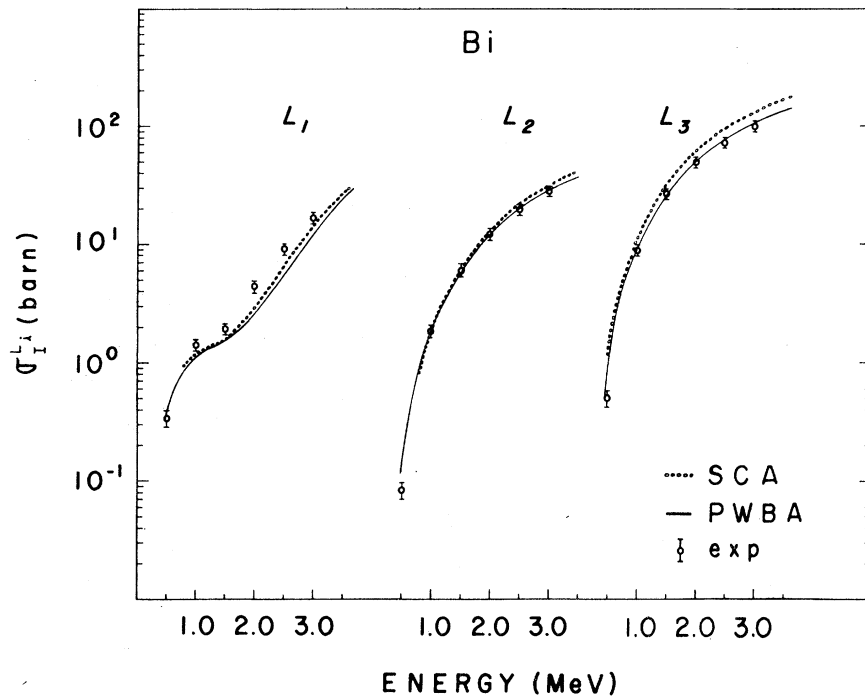
FIG. 6. Experimental ionization cross sections (open circles) for Bi vs proton energy. Also presented: PWBA and SCA theoretical curves.

the relativistic ionization cross sections are always larger than the nonrelativistic ones. On the other hand the $p_{3/2}$ state is less affected by the relativistic correction than the $p_{1/2}$ and $s_{1/2}$ states. This could explain, at least partially, the dis-

crepancies below 1 and 1.5 MeV in the gold and uranium regions, respectively. Rigorous calculations are not yet available for higher energies of the projectile. However the crude approximation given by Merzbacher and Lewis[1] points in the same
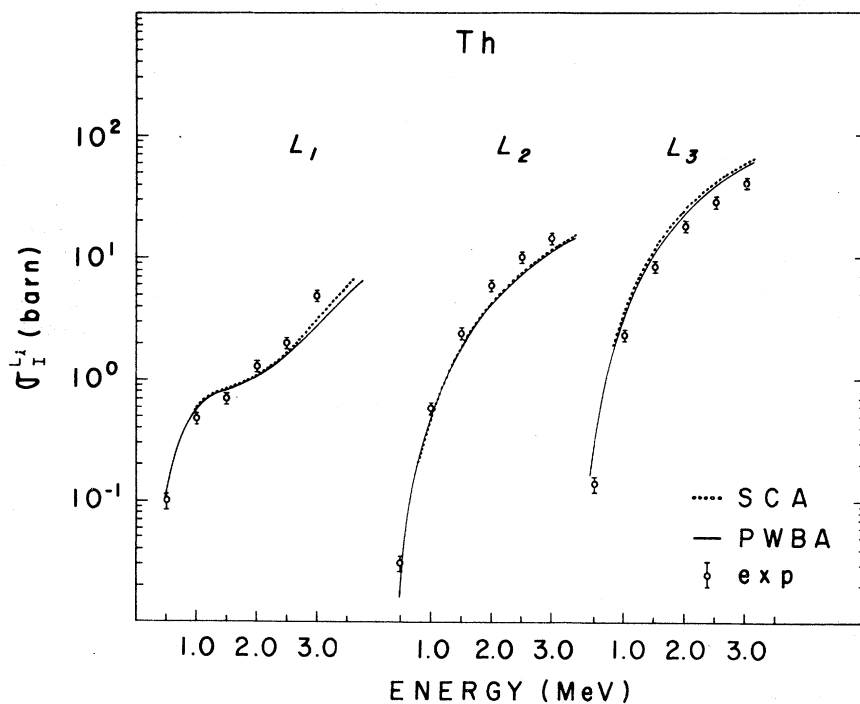


FIG. 7. Experimental ionization cross sections (open circles) for Th vs proton energy. Also presented: PWBA and SCA theoretical curves.
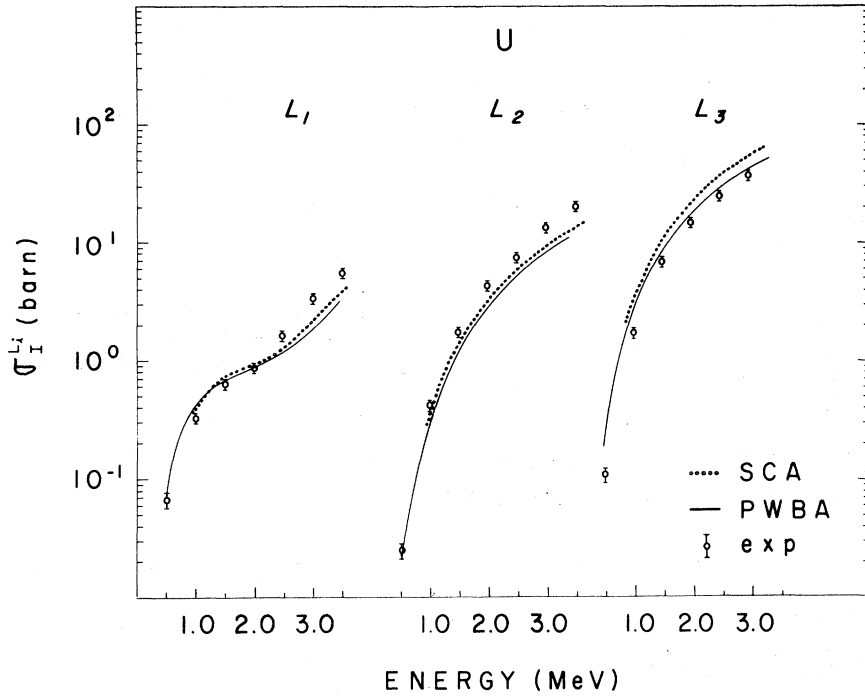
FIG. 8. Experimental ionization cross sections (open circles) for U vs proton energy. Also presented: PWBA and SCA theoretical curves.
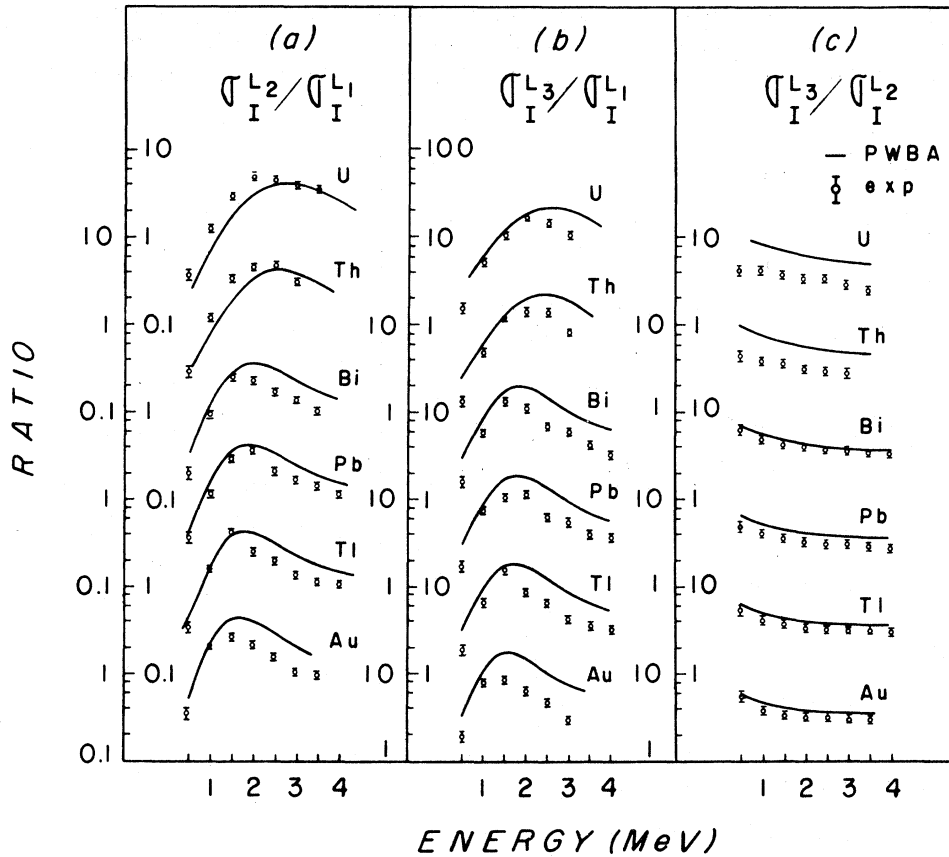


FIG. 9. Experimental $\sigma_I^{L2}/\sigma_I^{L1}$, $\sigma_I^{L3}/\sigma_I^{L1}$ and $\sigma_I^{L3}/\sigma_I^{L2}$ ratios (open circles) vs proton energy for Au, Tl, Pb, Bi, Th, and U. Also presented: PWBA curves.
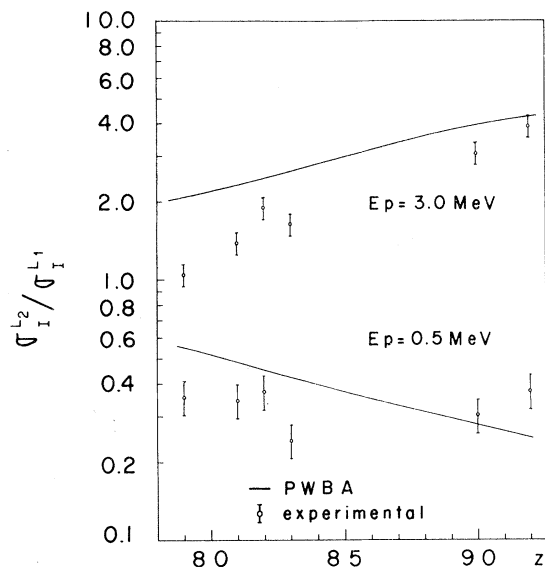
FIG. 10. The ratio $\sigma_I^{L2}/\sigma_I^{L1}$ as a function of $Z$ for $E_p$ = 0.5 and 3.0 MeV. The predictions of PWBA are also shown.

direction, namely, an increase in the cross sections and a small effect in the $L_3$ subshell for all the bombarding energies.

The behavior of $\sigma_I^{L2}/\sigma_I^{L1}$ and $\sigma_I^{L3}/\sigma_I^{L1}$ ratios are less regular. The general trend of the experimental points is the same as that exhibited by PWBA calculations, in particular a conspicuous maximum is well defined for all the elements. However, two main differences are observed when the experimental points are compared with the PWBA predictions: (i) the theoretical curves are displaced upwards (except, perhaps, $\sigma_I^{L2}/\sigma_I^{L1}$ for Th and U; (ii) the position of their maximum is, in general, shifted toward energies higher than the experimental position.

The $\sigma_I^{L2,L3}$ cross sections rise monotonically in the 0.5–3.0-MeV proton energy interval but this is not true for the $\sigma_I^{L1}$ cross sections. The $\sigma_I^{L1}(E)$ curve consists of two smooth increasing curves joined by a plateau whose position is $Z$ dependent. The existence of a pronounced maximum in the $\sigma_I^{L2,L3}/\sigma_I^{L1}$ ratios is a manifestation of this abrupt change in the slope of the $\sigma_I^{L1}(E)$ curve. However it must be emphasized that the position of the maximum do not coincide exactly with the position of center of the plateau.

The vertical displacement between data and theory is not so uniform as in the $\sigma_I^{L3}/\sigma_I^{L2}$ ratio. The plots of $\sigma_I^{L2,L3}/\sigma_I^{L1}$ as a function of $z$, for several energies do not show any simple systematic deviations between experimental and theoretical values. This is exemplified in Fig. 10, for the $\sigma_I^{L2}/\sigma_I^{L1}$ ratio at 0.5

and 3.0-MeV proton energies.

This vertical displacement is more evident above 1.5 MeV. An analysis of the expression (6), in which the numerical values are inserted, shows that in this region $f_{12}$ is less than the experimental error in the first term, and thus can be neglected in a first approximation. Because the PWBA curves are almost proportional to the experimental curves [Fig. 9(a) and 9(b)] in this energy region, the difference could be explained, at least partially, as a bad choice of the energy independent factor $\omega_{12}\Gamma_{21}\Gamma^{\gamma_4\gamma_1}$. However, the values of the $\omega_{12}$ ratio found in the literature are, in the extreme cases, only 20% higher than our adopted ratio. Errors in the branching ratios are typically of the same order of magnitude. Thus this argument is generally unable to explain differences between the experimental points and the theoretical curves which are higher than 40–50%.

It has been argued[31, 18, 20] that the plateau in the $\sigma_I^{L1}$ ionization cross section could be explained in terms of the momentum distribution of $2s$ electrons or, alternatively, in terms of the radial distribution of electron densities.[29] In fact both distributions present a node while the same distributions for $2p$ electrons are similar to those of $1s$ electrons, i.e., without nodes except at the origin. Merzbacher[31] showed that the ionization cross section at low energies is proportional to the square of the magnitude of the momentum distribution. The $2s$-state momentum distribution has a zero at $p = Z_L\hbar/2a_0$ (where $Z_L$ is the effective charge and $a_0$ the Bohr radius), presenting a large peak for lower and a smaller peak for higher momenta. Consequently a smoothing is expected to occur in the ionization cross section at a fixed value of $\eta_L/\theta_L^2$, where $\eta_L$ and $\theta_L$ are the dimensionless parameters defined in Ref. 1:

$$\eta_L = \frac{1}{Z_L^2}\left(\frac{\hbar v}{e^2}\right)^2$$

and

$$\theta_L = \frac{4I_L}{Z_L^2 R_\infty} \; ;$$

$v$ being the projectile velocity relative to the target atom, $I_L$ the measured binding energy, and $R_\infty$ the Rydberg constant.

The fact that the $\sigma_I^{L2,L3}/\sigma_I^{L1}$ ratios are less than 1 at low energies reflects special features of the momentum distributions, namely, the fact that the $2s$ secondary peak at high momenta dominates the $2p$ momentum amplitudes.

Alternatively the same situation can be visualized in configuration space, as proposed by Hansteen.[18] If $b_{max}$ represents the impact parameter
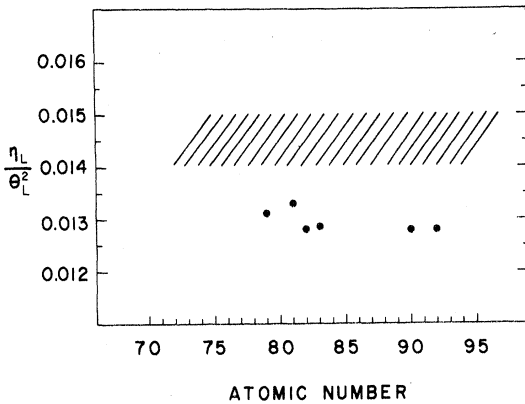
FIG. 11. The value of the dimensionless parameter $\eta_L/\Theta^2_L$ at the position of the center of the plateau vs the atomic number. The hatched band corresponds to the PWBA predictions and the circles are from the experiment.

that gives the maximum contribution to the total Coulomb ionization cross section then $b_{max} \approx \hbar v/\Delta E$, where $\Delta E \sim I_L$ is the energy transfered to the atom in the collision. A correlation is observed between the density nodes and the dominant impact parameters extracted from the approximate position of the plateau in $\sigma^{L_1}_I$ curves. It is noteworthy that the density nodes from Hartree-Fock calculations[32] occur systematically nearer the origin than those obtained from hydrogenic wave functions. The shift amounts to 3.7% (which corresponds to two or three units in the effective charge) and could explain the shift in the position of the maximum in the $\sigma^{L_2, L_3}_I/\sigma^{L_1}_I$ curves as compared with PWBA predictions since calculations are performed with nonrelativistic hydrogenic wave functions. Relativistic corrections would reinforce the effect.

Figure 11 indicates the $\eta_L/\theta^2_L$ values correspondent to the center of the plateau as given by PWBA
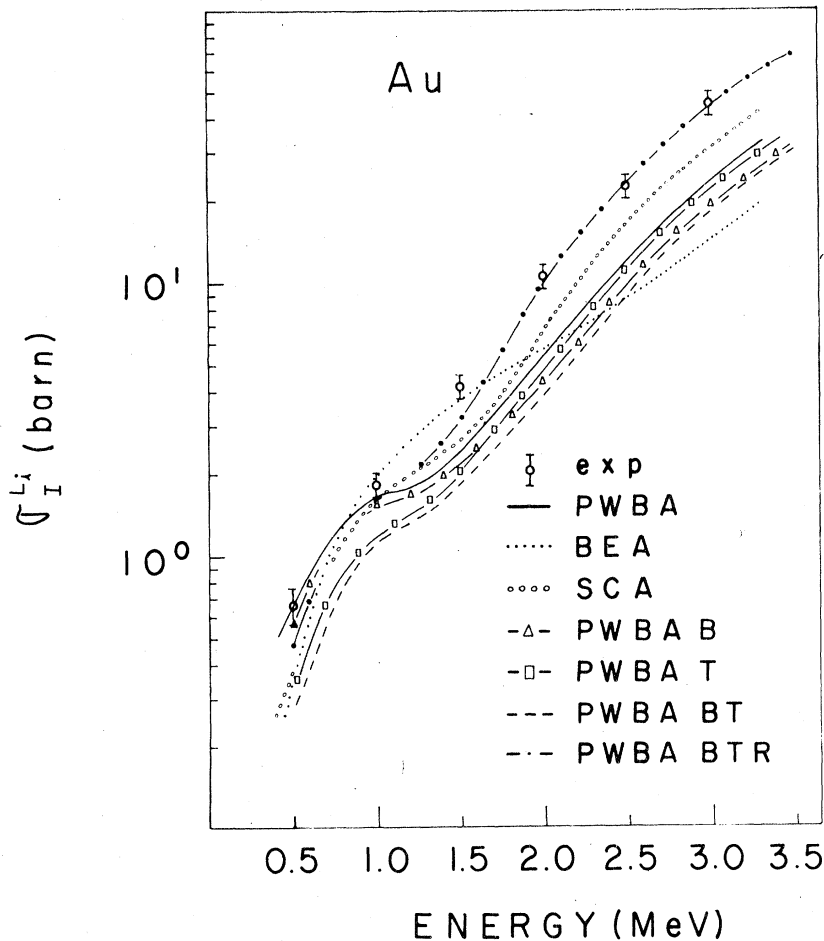


FIG. 12. Comparison between the experimental $\sigma^{L_1}_I$ cross sections for Au and theoretical curves: PWBA, PWBA with binding correction (PWBA-B), PWBA with trajectory correction (PWBA-T), PWBA with binding and trajectory correction (PWBA-BT), PWBA with binding, trajectory and relativistic corrections (PWBA-BRT), SCA and BEA.
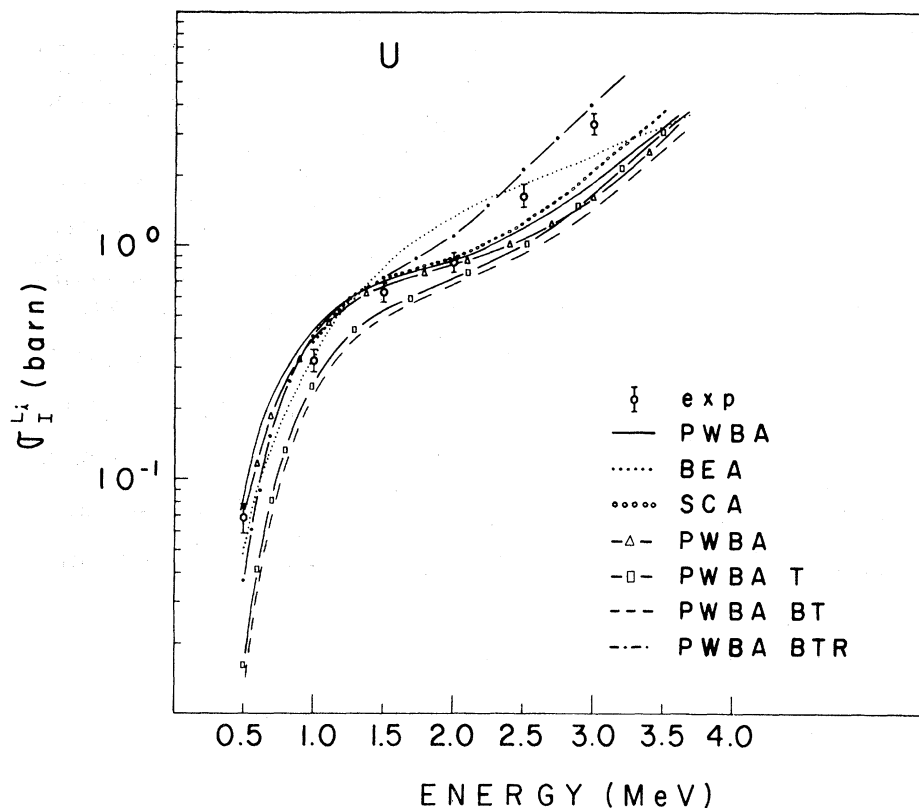
FIG. 13. Comparison between the experimental $\sigma_I^{L_1}$ cross sections for U and theoretical curves: PWBA, PWBA with binding correction (PWBA-B), PWBA with trajectory correction (PWBA-T), PWBA with binding and trajectory correction (PWBA-BT), PWBA with binding trajectory and relativistic corrections (PWBA-BRT), SCA and BEA.

calculations (the hatched band from 0.014 to 0.015) and the same values as given by experiment.

There is an obvious possibility of some underlying correlation between the position of the plateau and the existence of a node in $2s_{1/2}$ momentum or configuration space wave functions.

Figures 12 and 13 presents the $L_I$ PWBA predictions for Au and U, respectively, including corrections for the hyperbolic trajectory of the proton,[17] the effect of the changing binding energy of the target electron,[17] and relativistic corrections.[1] The BEA and SCA calculations are also shown in Figs. 12 and 13. The large value of each of the

corrections invalidates quantitative conclusions regarding agreement between experimental and theoretical values. We believe that these approximations are probably too simplified to predict correctly the ionization cross sections in this energy range even if reasonable fits are occasionally achieved.

[1]E. Merzbacher and H. W. Lewis, *Encyclopedia of Physics* (Springer-Verlag, Berlin, 1958), Vol. 34, p. 166.
[2]T. B. Johansson, R. Akselsson, and S. A. E. Johansson, Nucl. Instrum. Methods 84, 141 (1970).
[3]C. G. Soares, R. D. Lear, J. T. Sanders, and H. A. Van Rinsvelt, Phys. Rev. A 13, 953 (1976).
[4]J. H. Scofield, Phys. Rev. 179, 9 (1969).
[5]J. H. Scofield, Phys. Rev. A 10, 1507 (1974).
[6]H. R. Rosner and C. P. Bhalla, Z. Phys. 231, 347
(1970).
[7]E. J. McGuire, Phys. Rev. A 3, 587 (1971).
[8]M. H. Chen, B. Crasemann, and V. O. Kostroun, Phys. Rev. A 4, 1 (1971).
[9]W. Bambynek, B. Crasemann, R. W. Fink, H. U. Freund, H. Mark, C. D. Swift, R. E. Price, and P. Venugopala Rao, Rev. Mod. Phys. 44, 717 (1972).
[10]A. G. de Pinho and M. Weksler, Z. Naturforsch. 28A, 1635 (1973).
[11]A. G. de Pinho, L. T. Auler, and A. G. da Silva, Phys. Rev. C 9, 2056 (1974).
[12]M. Weksler and A. G. de Pinho, Rev. Bras. Fis. 3, 291 (1973).

[13]L. T. Auler, A. G. da Silva, and A. G. de Pinho, Rev. Bras. Fis. 4, 29 (1974).

[14]S. Datz, V. L. Duggan, L. C. Feldman, E. Laesgsgaard, and J. U. Andersen, Phys. Rev. A 9, 192 (1974).

[15]H. Tawara, K. Ishii, S. Morita, H. Kaji, and T. Shiokawa, Phys. Rev. A 11, 1560 (1975).

[16]W. Brandt and G. Lapicki, Phys. Rev. A 10, 474 (1974).

[17]G. H. Pepper, Ph. D. thesis (North Texas State University, 1974) (unpublished).

[18]J. M. Hansteen and O. P. Mosebekk, Nucl. Phys. A 201, 541 (1973); see also J. M. Hansteen, Scientific Report 79, University of Bergen, 1975 (unpublished).

[19]J. H. McGuire and K. Omidvar, Phys. Rev. A 10, 182 (1974).

[20]A. E. Kingston, J. Phys. B 3, L45 (1970).

[21]R. C. Bearse, D. A. Close, J. J. Malanify, and C. J. Umbarger, Phys. Rev. A 7, 1269 (1973).

[22]S. M. Shafroth and G. A. Bissinger, Phys. Rev. A 7, 566 (1973).

[23]R. Akselsson and T. B. Johansson, Z. Phys. 266, 245 (1974).

[24]H. Tawara, K. Ishii, S. Morita, H. Kaji, C. N. Shu, and T. Shiokawa, Phys. Rev. A 9, 1617 (1974).

[25]C. V. Barros Leite, A. G. de Pinho, and N. V. de Castro Faria (unpublished).

[26]S. I. Salem and C. W. Schultz, At. Data 3, 215 (1971).

[27]L. Salgueiro, M. T. Ramos, M. L. Escrivão, M. C. Martins, and J. G. Ferreira, J. Phys. B 7, 342 (1974).

[28]B. H. Choi, Phys. Rev. A 4, 1002 (1971).

[29]C. F. Fischer, At. Data 4, 301 (1972).

[30]C. N. Chang, J. F. Morgan, and S. L. Blatt, Phys. Rev. A 11, 607 (1975).

[31]E. Merzbacher, *Proceedings of the International Conference on Inner Shell Ionization Phenomena and Future Applications*, CONF-720404, (Natl. Tech. Information Service, Springfield, Va., 1972), Vol. 2, p. 915.

[32]C. F. Fischer, At. Data 4, 302 (1972).

[33]C. N. Chang, J. F. Morgan, and S. L. Blatt, quoted in Ref. 37.

[34]E. M. Berstein and H. W. Lewis, Phys. Rev. 95, 83 (1954).

[35]C. E. Busch, A. B. Baskin, P. H. Nettles, and S. M. Shafroth, Phys. Rev. A 7, 1601 (1973).

[36]T. K. Li, D. L. Clark, and G. W. Greenless, quoted in Ref. 37.

[37]T. L. Hardt and R. L. Watson, At. Data Nucl. Data Tables 17, 107 (1976).